Supporting Information

An anisotropically crystallized and nitrogen-doped $CuWO_4$ photoanode for efficient and robust visible-light-driven water oxidation

Tomohiro Katsuki, Zaki N. Zahran, Norihisa Hoshino, Yuta Tsubonouchi, Debraj Chandra, and Masayuki Yagi*

Department of Materials Science and Technology, Faculty of Engineering, Niigata University, 8050 Ikarashi-2, Niigata 9050-2181, Japan.

*Correspondence to: yagi@eng.niigata-u.ac.jp

Contents

Table S1. Comparison of performances of state-of-the-art $CuWO_4$-based photoanodes for PEC water oxidation.[a)]

Sample	Synthesis	Buffer	pH	$j_{1.23}$ / mA cm^{-2}	$IPCE_{420}$ (%)	η_{sep} (%)	η_{cat} (%)	FE_{O2} (%)	Stability: Remaining photocurrent (%) (reaction time)	Ref.
N-$CuWO_4$	MiMIC	0.1 M KPi	7.0	0.21	5.6	12.3 [b)]	51.9 [b)]	97 [c)]	92 (40 h) [c)]	This work
$CuWO_4$ nanoflake	Sacrificial templates	1.0 M KBi	9.5	0.4	8	12	55	nr	100 (5 h)	R1
$CuWO_4$ nanoflake	Sacrificial templates	0.1 M KPi	7.0	0.3	nr	nr	nr	nr	95 (1 h)	R2
$CuWO_4$ nanoflake	Sacrificial templates	0.2 M Na_2SO_4	7.0	0.09	nr	10.8	15.8	nr	45 (6 h)	R3
$CuWO_4$ with oxygen vacancy	Sacrificial templates	0.2 M Na_2SO_4	7.0	0.2	nr	11.2	26.2	nr	60 (6 h)	R3
$CuWO_4$	Ultrasonic spray pyrolysis	0.2 M Na_2SO_4	6.4	0.033	nr	nr	nr	nr	96 (2100 s)	R4
$CuWO_4$ on carbon nanotube	Spray pyrolysis	0.25 M ($NaHCO_3$/Na_2CO_3)	10.0	0.23	7[d)]	nr	nr	nr	85 (24 h)[d)]	R5
$CuWO_4$	Spray pyrolysis	0.1 M KPi	7.0	0.13	< 1	2.5	25	nr	nr	R6
$CuWO_4$	Spray pyrolysis	0.1 M KBi	7.0	0.08	nr	nr	nr	nr	nr	R7
$CuWO_4$	Spin-coating	0.5 M KBi with 0.2M KCl	7.0	0.1	nr	nr	nr	nr	nr	R8
$CuWO_4$	Spin-coating	0.1 M KPi	7.0	0.15	nr	nr	nr	100	15 (12 h)	R9
$CuWO_4$	Spin-coating	0.1 M KBi	7.0	0.10	nr	nr	nr	96	93 (12 h)	R9
$CuWO_4$	Spin-coating	0.1 M Na_2SO_4	6.8	0.267	2	nr	nr	nr	nr	R10
Nodular $CuWO_4$	Electrochemical deposition	0.1 M KPi	7.0	0.072	21 [e)]	nr	nr	> 90	nr	R11

$CuWO_4$	Electrochemical deposition	0.1 M KPi	7.0	0.026	0.2	nr	nr	nr	81 (150 s)	R12
$CuWO_4$ nanoparticle	Spray pyrolysis	0.1 M KPi	7.0	0.03	2	nr	nr	nr	50 (4000 s)	R13
$CuWO_4$	Spray pyrolysis	0.3 M KBi	7.5	0.027	0.03	nr	nr	nr	nr	R14
N_2-treated $CuWO_4$	Electrochemical deposition	0.1 M KPi	7.0	0.08	nr	4	nr	nr	nr	R15
H_2-treated $CuWO_4$	Hydrothermal	0.1 M Na_2SO_4	6.8	0.2	nr	nr	nr	nr	75 (1 h) [e)]	R16
$CuWO_4$ nanoparticle	Electrochemical deposition	0.1 M KPi	7.0	0.015	0.2	1.5	23	nr	nr	R17
Porous $CuWO_4$	Electrochemical deposition	0.1 M KPi	7.0	0.2	nr	nr	nr	nr	~80 (12 h) [f)]	R18
$CuWO_4$ with a predominant (100) facet	Hydrothermal	0.2 M KPi	~7	0.38	11	20.4	26.2	75	85 (6 h)	R19
Polycrystalline CuWO4	RF magnetron sputtering	0.33 M H_3PO_4	1.35	0.126	nr	nr	nr	nr	nr	R20
$CuWO_4$	Spray pyrolysis	0.1 M KPi	7.0	0.5	nr	nr	nr	nr	~80 (10 h)	R21

[a)] nr: not reported, measured at 1.23V vs. RHE with simulated solar light (AM 1.5, 100 mW cm^{-2}), [b)] monoclinic light (LED, 420 nm, 3.78 mW cm^{-2}), [c)] visible light (Xe lamp with L39 and heat-cut filter, 100 mW cm^{-2}), [d)] at 1.63 V vs. RHE, [e)] at 1.6 V vs. RHE, [f)] at 1.1 V vs. RHE.

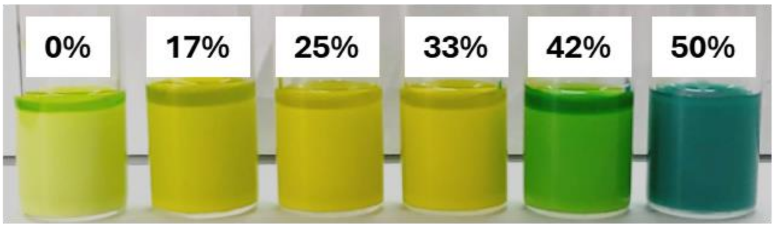

Figure S1 Photos of precursor suspensions containing 0.42 M $Cu(NO_3)_2$ and 0.50 M WCl_6 with different fractions (F_{im} = 0 ~ 50% vol) of BIm in methanol/BIm mixed solvents. F_{im} values are indicated on the figure.

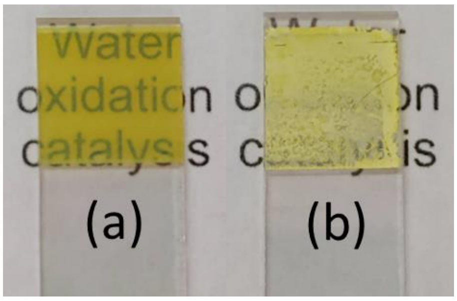

Figure S2 Photos of $CuWO_4$ films with F_{im} of (a) 33% and (b) 0% on an FTO substrate.

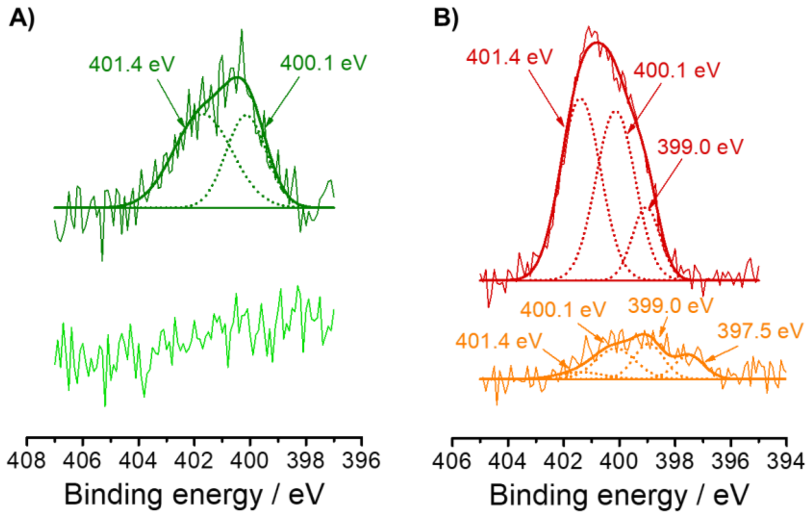

Figure S3. XPS spectra in the N1s region for $CuWO_4$ films with F_{im} of (A) 0% and (B) 33% before (top) and after (bottom) a surface treatment with Ar plasma etching.

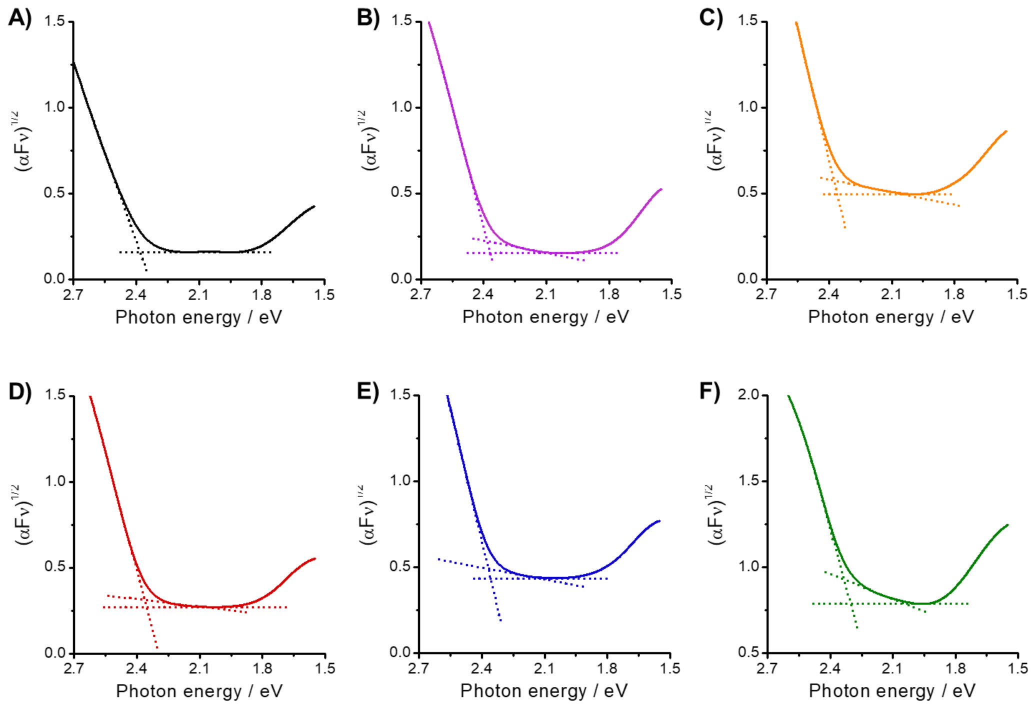

Figure S4 Tauc plots based on the DRS spectra (Figure 4A) of $CuWO_4$ films with F_{im} of (A) 0%, (B) 17%, (C) 25%, (D) 33%, (E) 42% and (F) 50%. The dotted lines represent slopes to calculate bandgap energies.

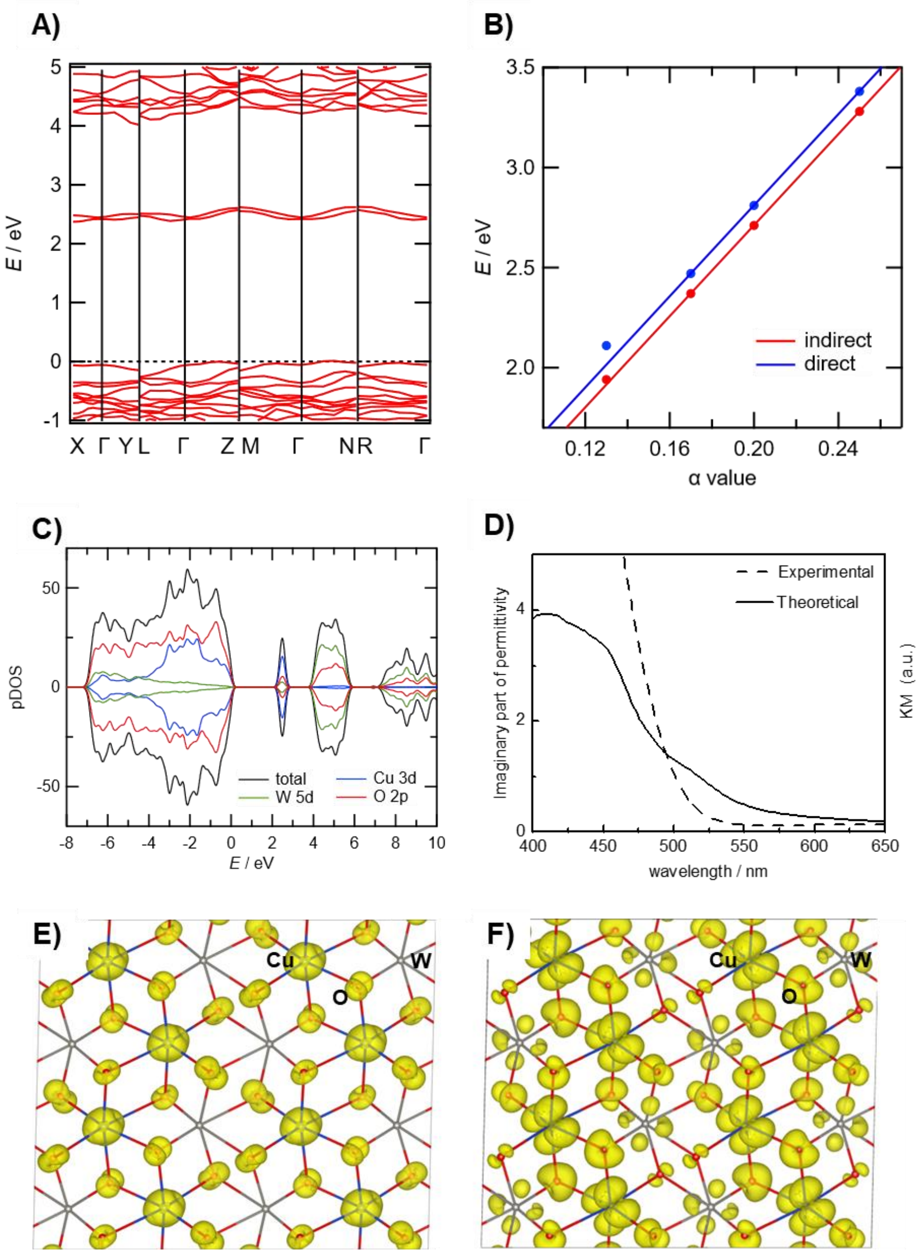

Figure S5 (A) Band diagram calculated for neat $CuWO_4$ crystals using HSE06 functional with the exact exchange mixing coefficient (α) of 0.17. (B) Plots of the calculated band gap versus α values. (C) pDOS diagram (black) calculated for neat $CuWO_4$ at $\alpha = 0.17$. Contributions from the Cu 3d (blue), O 2p (red) and W 5d (green) bands are indicated by different colors. (D) Imaginary part of the calculated dielectric coefficients (solid line) and the measured DRS spectrum for neat-$CuWO_4$ (dashed line). Integrated density of states (IDOS) of (E) the valence band (VB) top and (F) the conduction band (CB) bottom for neat $CuWO_4$. The atoms of Cu, O, and W are marked in figures.

Table S2. Parameters for calculation of replacement energies ($E_{rep}(\Delta\varepsilon_F)$) of O1-O4 with N^{1-}, N^{2-}, and N^{3-} for $CuWO_4$.

dopant	site	q	$E_{rep}(0)$
N^{1-}	O1	+1	3.59
	O2	+1	3.83
	O3	+1	3.82
	O4	+1	3.69
N^{2-}	O1	0	4.26
	O2	0	4.83
	O3	0	4.67
	O4	0	4.38
N^{3-}	O1	−1	4.93
	O2	−1	5.35
	O3	−1	5.05
	O4	−1	5.18

Table S3. Summary of energy levels of VB top and CB bottom, impurity bands, and transition energies estimated from the PDOS diagrams. [a]

Dopant	Site	Spin	E_{VB} / eV	E_{N-d} / eV	E_{N-a} / eV	E_{CB} / eV	Transition energy / eV (Assignment)
Neat		up	−0.42			1.95	2.37 (VB → CB)
		down	−0.42			1.95	2.37 (VB → CB)
N^{1-}	O1	up	0.00			2.25	2.25 (VB → CB)
			0.00		1.32		1.32 (VB → N-a1)
		down	0.00			2.33	2.33 (VB → CB)
			0.00		2.14		2.14 (VB → N-a2)
			0.00		1.47		1.47 (VB → N-a3)
	O2	up	0.00			2.23	2.23 (VB → CB)
		down	0.00			2.31	2.31 (VB → CB)
					1.97		1.97 (VB → N-a1)
					1.67		1.67 (VB → N-a2)
	O3	up	−0.14			2.10	2.24 (VB → CB)
				−0.03		2.10	2.13 (N-d1 → CB)
		down	−0.09			2.22	2.19 (VB → CB)
			−0.09		1.71		1.80 (VB → N-a1)
	O4	up	0.00			2.34	2.34 (VB → CB)
			0.00		2.21		2.21 (VB → N-a1)
			0.00		1.41		1.41 (VB → N-a2)
		down	0.00			2.32	2.32 (VB → CB)
			0.00		1.47		1.47 (VB → N-a1)
N^{2-}	O1	up	−0.29			2.00	2.30 (VB → CB)
				−0.01			2.02 (N-d1 → CB)
		down	−0.33			2.02	2.36 (VB → CB)
				−0.21		2.02	2.24 (N-d1 → CB)
			−0.33		1.86		2.19 (VB → N-a1)
	O2	up	−0.57			1.71	2.28 (VB → CB)
				−0.45		1.71	2.16 (N-d1 → CB)
		down	−0.57			1.68	2.25 (VB → CB)
			−0.57		1.38		1.95 (VB → N-a1)
				−0.10		1.68	1.78 (N-d1 → CB)
				0.00		1.68	1.68 (N-d2 → CB)
				−0.10	1.38		1.48 (N-d1 →N-a1)
				0.00	1.38		1.38 (N-d2 → N-a2)
	O3	up	−0.42			1.85	2.27 (VB → CB)
				−0.28		1.85	2.16 (N-d1 → CB)
		down	−0.44			1.85	2.29 (VB → CB)
				−0.01		1.85	1.86 (N-d1 → CB)
			−0.44		1.19		1.63 (VB → N-a1)
				−0.01	1.19		1.20 (N-d1 →N-a1)
	O4	up	−0.20			2.12	2.32 (VB → CB)
				−0.02		2.12	2.14 (N-d1 → CB)
		down	−0.15	-		2.10	2.25 (VB → CB)

Table S3. (continued)

Dopant	Site	Spin	E_{VB}	$E_{N\text{-}d}$	$E_{N\text{-}a}$	E_{CB}	Transition energy (assignment)
N^{3-}	O1	up	−0.59			1.73	2.32 (VB → CB)
				−0.43		1.73	2.16 (N-d1 → CB)
				−0.20		1.73	1.93 (N-d2 → CB)
				−0.09		1.73	1.82 (N-d3 → CB)
		down	−0.59			1.73	2.32 (VB → CB)
				−0.44		1.73	2.17 (N-d1 → CB)
				−0.01		1.73	1.74 (N-d2 → CB)
	O2	up	−0.53			1.79	2.32 (VB → CB)
				−0.31		1.79	2.10 (N-d1 → CB)
				−0.14		1.79	1.93 (N-d2 → CB)
		down	−0.50			1.74	2.24 (VB → CB)
				−0.18		1.74	1.92 (N-d1 → CB)
				−0.08		1.74	1.82 (N-d2 → CB)
				−0.01		1.74	1.75 (N-d3 → CB)
	O3	up	−0.58			1.74	2.33 (VB → CB)
				−0.40		1.74	2.14 (N-d1 → CB)
				−0.31		1.74	2.05 (N-d2 → CB)
				−0.19		1.74	1.93 (N-d3 → CB)
		down	−0.53			1.74	2.28 (VB → CB)
				−0.18		1.74	1.92 (N-d1 → CB)
				−0.01		1.74	1.75 (N-d2 → CB)
	O4	up	−0.52			1.73	2.26 (VB → CB)
				−0.32		1.73	2.05 (N-d1 → CB)
				−0.09		1.73	1.83 (N-d2 → CB)
		down	−0.50			1.73	2.24 (VB → CB)
				−0.01		1.73	1.73 (N-d1 → CB)

[a] E_{VB}, E_{VB}, $E_{N\text{-}d}$ and $E_{N\text{-}a}$ are energy levels of VB top, CB bottom, donor and acceptor impurity bands due to N 2p orbitals, respectively.

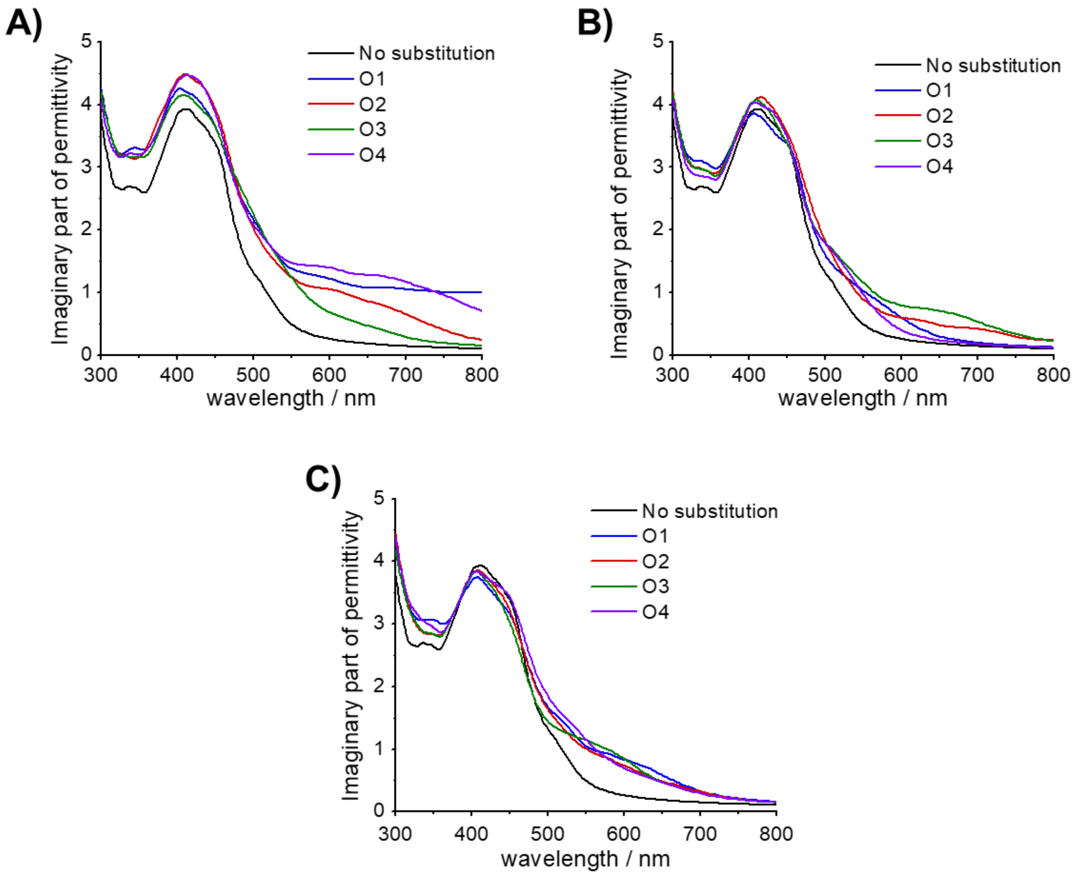

Figure S6. Imaginary part of the calculated dielectric coefficients for neat-$CuWO_4$ (black) and N-$CuWO_4$ with substitutions of O1-O4 with (A) N^{1-}, (B) N^{2-}, and (C) N^{3-} . The replaced O atoms in O1-O4 are indicated by different colors in each figure.

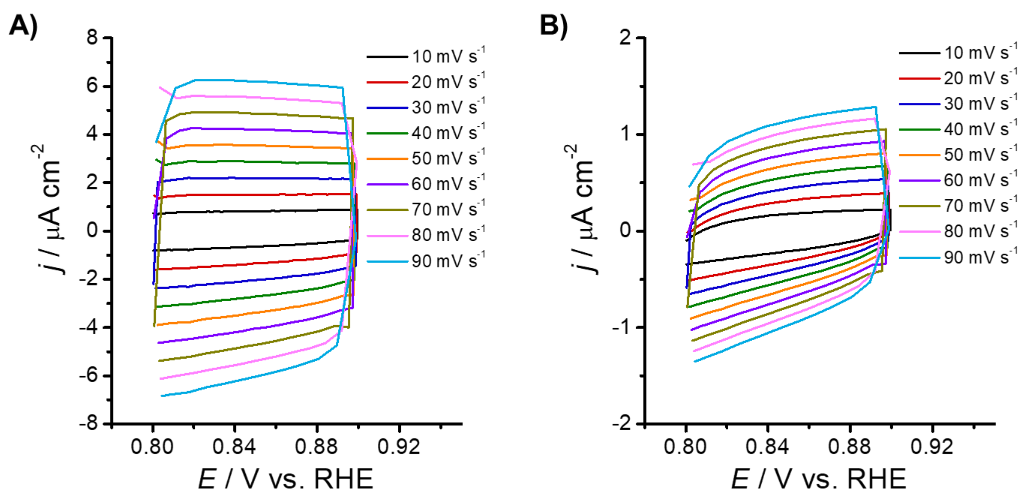

Figure S7 CVs of (A) N-$CuWO_4$ (F_{im} = 33%) and (B) neat-$CuWO_4$ electrodes as measured in 0.1 M KPi solutions (pH = 7) in the potential range of 0.8 – 0.9 V vs. RHE at different scan rates of 10 – 90 mV s^{-1} under dark conditions.

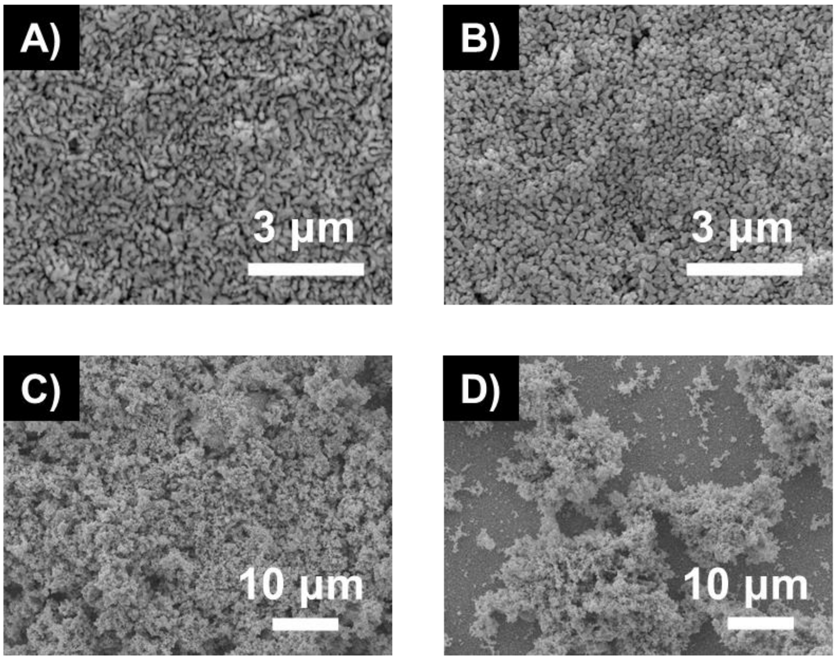

Figure S8 Top view SEM images of (A and B) N-$CuWO_4$ (F_{im} = 33%) and (C and D) neat-$CuWO_4$ electrode (A and C) before and (B and D) after 15 h photoelectrolysis in a 0.1 M KPi buffer (pH 7.0) at 1.23 V under the light irradiation (>390 nm, 100 mW cm^{-2}).

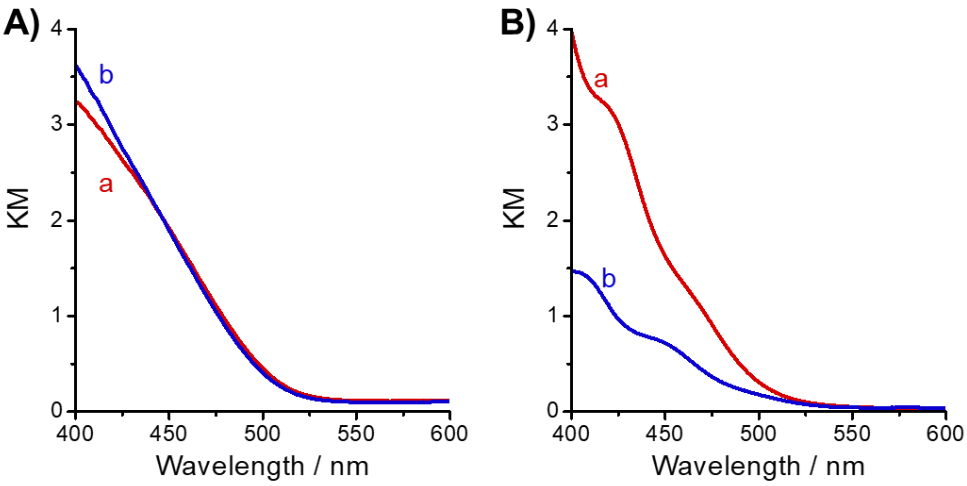

Figure S9 DRS of (A) N-$CuWO_4$ (F_{im} = 33%) and (B) neat-$CuWO_4$ electrodes before (a, red) and after 15 h photoelectrolysis (b, blue) in a 0.1 M KPi buffer (pH 7.0) at 1.23 V under the light irradiation (>390 nm, 100 mW cm^{-2}).

Reference

R1 W. Ye, F. Chen, F. Zhao, N. Han and Y. Li, *ACS Appl. Mater. Interfaces*, 2016, **8**, 9211–9217.

R2 D. Hu, P. Diao, D. Xu, M. Xia, Y. Gu, Q. Wu, C. Li and S. Yang, *Nanoscale*, 2016, **8**, 5892–5901.

R3 W. Guo, Y. Wang, X. Lian, Y. Nie, S. Tian, S. Wang, Y. Zhou and G. Henkelman, *Catal. Sci. Technol.*, 2020, **10**, 7344–7351.

R4 X. Duan, C. Xu, A. M. El Nahrawy, J. Chen, Z. Zhu, J. Wang, Q. Liang and F. Cao, *ChemNanoMat*, 2022, **8**.

R5 N. Gaillard, Y. Chang, A. Deangelis, S. Higgins and A. Braun, *Int. J. Hydrogen Energy*, 2013, **38**, 3166–3176.

R6 D. Bohra and W. A. Smith, *Phys. Chem. Chem. Phys.*, 2015, **17**, 9857–9866.

R7 C. R. Lhermitte and B. M. Bartlett, *Acc. Chem. Res.*, 2016, **49**, 1121–1129.

R8 K. J. Pyper, J. E. Yourey and B. M. Bartlett, *J. Phys. Chem. C*, 2013, **117**, 24726–24732.

R9 J. E. Yourey, K. J. Pyper, J. B. Kurtz and B. M. Bartlett, *J. Phys. Chem. C*, 2013, **117**, 8708–8718.

R10 Y. Sun, F. Du, D. Xie, D. Yang, Y. Jiao, L. Jia and H. Fan, *Chin. Phys. B*, 2020, **29**, 127801.

R11 J. C. Hill, Y. Ping, G. A. Galli and K. S. Choi, *Energy Environ. Sci.*, 2013, **6**, 2440–2446.

R12 M. Davi, M. Mann, Z. Ma, F. Schrader, A. Drichel, S. Budnyk, A. Rokicinska, P. Kustrowski, R. Dronskowski and A. Slabon, *Langmuir*, 2018, **34**, 3845–3852.

R13 M. Valenti, D. Dolat, G. Biskos, A. Schmidt-Ott and W. A. Smith, *J. Phys. Chem. C*, 2015, **119**, 2096–2104.

R14 A. Venugopal and W. A. Smith, *Faraday Discuss.*, 2019, **215**, 175–191.

R15 Z. Ma, O. Linnenberg, A. Rokicinska, P. Kustrowski and A. Slabon, *J. Phys. Chem. C*, 2018, **122**, 19281–19288.

R16 Y. Tang, N. Rong, F. Liu, M. Chu, H. Dong, Y. Zhang and P. Xiao, *Appl. Surf. Sci.*, 2016, **361**, 133–140.

R17 M. Davi, A. Drichel, M. Mann, T. Scholz, F. Schrader, A. Rokicinska, P. Kustrowski, R. Dronskowski and A. Slabon, *J. Phys. Chem. C*, 2017, **121**, 26265–26274.

R18 J. E. Yourey and B. M. Bartlett, *J. Mater. Chem.*, 2011, **21**, 7651.

R19 L. Chen, W. Li, W. Qiu, G. He, K. Wang, Y. Liu, Q. Wu and J. Li, *ACS Appl. Mater. Interfaces*, 2022, **14**, 47737–47746.

R20 Y. Chang, A. Braun, A. Deangelis, J. Kaneshiro and N. Gaillard, *J. Phys. Chem. C*, 2011, **115**, 25490–25495.

R21 C. M. Tian, M. Jiang, D. Tang, L. Qiao, H. Y. Xiao, F. E. Oropeza, J. P. Hofmann, E. J. M. Hensen, A. Tadich, W. Li, D. C. Qi and K. H. L. Zhang, *J. Mater. Chem. A*, 2019, **7**, 11895–11907.